Tellus (1994), 46B, 325–338
Printed in Belgium – all rights reserved

TELLUS
ISSN 0280–6509

The sizes of the jet drops produced by air bubbles bursting on sea- and fresh-water surfaces

By DONALD E. SPIEL, *Department of Physics, Naval Postgraduate School, Monterey, California 93943, USA*

(Manuscript received 1 October 1993; in final form 3 February 1994)

ABSTRACT

The size distributions of the top 6 jet drops produced by air bubbles bursting on sea- and fresh-water surfaces are presented for bubbles with radii from 350 to 1500 μm. There are no significant differences in the results between sea- and fresh-water. Except for the top drop, the size distributions are often bimodal. For the top jet drop, the dependence of the average droplet radius, R_d, on bubble radius, R_b, is given by the fit $R_d = 0.0337\ R_b^{1.208}$ (μm) which compares well with the results for the top drop reported by Blanchard in 1989. Excluding the droplets in the small modes, the droplet size dependence on bubble size for the lower droplets (those subsequent to the top drop) is, within statistical certainty, the same for all the droplets from the second through the fifth. The data for these droplets is fit by $R_d = 0.0165\ R_b^{1.325}$. The probability that a bubble with a given radius produces at least n drops is given for n up to 7, although a small number of bubble bursts were observed to have produced at least 15 jet droplets.

1. Introduction

The aerosols which result from bubbles bursting on the surface of the sea are known to have an important role in air–sea interactions (Blanchard, 1963, 1983; Blanchard and Woodcock, 1957; Coantic, 1980; Coantic et al., 1981; Katsaros et al., 1987, Kerman, 1984; Larsen et al., 1990; Merlivat and Memery, 1983; Monahan and Spillane, 1984; Woodcock, 1952), in the transport of microorganisms (Blanchard and Syzdek, 1972; Woodcock, 1953), and optical transmission in the lower marine atmosphere boundary (De Leeuw, 1991; Schacher et al., 1981). The mechanics of bubble bursting has been widely studied (Afeti and Resch, 1990; Blanchard, 1958, 1963, 1989, 1990; Blanchard and Syzdek, 1975, 1988; Coantic, 1980; Coantic et al., 1981; Day, 1964; Dekker and De Leeuw, 1993; Detwiler and Blanchard, 1978; Kientzler et al., 1954; MacIntyre, 1972; Resch et al., 1986; Resch and Afeti, 1991, 1992; Spiel, 1992; Toba, 1959; Woodcock et al., 1953). In order to understand and to model this air–sea interaction it is vital to determine the details of the bursting of single bubbles. Modelers of the air–sea interaction process, for example, require a knowledge of the number and size distribution, as well as the initial velocities, of the droplets from single bursting bubbles (Burk, 1984; De Leeuw, 1987; Mestayer et al., 1989; Mestayer and Lefauconnier, 1988; Stramska, 1987; Rouault et al., 1991).

A collapsing bubble can, depending on its size, create aerosols by two distinct mechanisms. The first aerosols to emerge are the so-called film droplets which originate from the disruption of the bubble cap by rapid movement of the torn cap edges and the escaping bubble gas. See Afeti and Resch (1990), Resch and Afeti (1991) and Resch et al. (1986) for dramatic photographs of the film drop production process. Only bubbles with diameters larger than about 1 mm produce these film drops (Blanchard and Syzdek, 1988). The second mechanism for droplet generation arises as a result of the surface tension accelerating the surface in a boundary layer shear flow down the cavity wall as discussed by MacIntyre (1972). As

the water converges at the bottom of the cavity opposing jets are created. The upward jet is unstable and usually breaks up into a number of droplets called jet drops. Kientzler et al. (1954) used high speed cameras to show the rising jet and its breakup.

Data relating jet drop size to bubble size, as reviewed by Blanchard (1989), has been meager. This paper provides some of the needed data by presenting the results of measurements of the number and size distributions of the jet drops produced by single collapsing bubbles of known size. The data gathered permitted the determination of both the ejection time and ejection speed in addition to the size of the droplets, but only limited results of ejection speeds will be presented here. In the next section the equipment and experiment design will be discussed. Section 3 will present the results and compare them to earlier measurements. The final section will offer a summary and discuss future plans.

2. Equipment of procedures

The experimental arrangement is illustrated in Fig. 1. Bubbles, generated by forcing air through glass capillaries, were made one at a time on demand. The Helmholtz signal emitted by a bursting bubble (Spiel, 1992), detected by a microphone offset from the vertical, as shown, is used to trigger the subsequent accumulation of data. The Helmholtz signal not only provides this $t=0$ reference, but a measure of the bubble size as well. A second detector, located directly above the collapsing bubble, is used to detect the impinging droplets. This apparatus, cleaning procedures, and bubble size measurements were described by Spiel (1992).

The jet droplet sizes were determined using a Particle Measuring Systems, Inc., model OAP-260X optical array probe (OAP). The OAP uses a laser in conjunction with a 64-element linear array of photodetectors to detect and size the droplets as illustrated in Fig. 2. A droplet transiting the beam casts its shadow on the array of photodetectors and the number of array elements shadowed is translated into a bin size. For the particular OAP model used in these studies there are 62 size bins which are 5 μm radius wide. The sizes at the centers of these 62 bins are set by the magnification of the optics and range from 6 to 310 μm radius for this particular instrument. Thus, particles whose actual radii are within ± 2.5 μm of a bin center fall into that bin and will be considered as having that bin center size. The OAP has been modified so that, in addition to sizing a particle, it provides the information necessary to determine the time of droplet passage and the average speed of the particle over a distance equal to its diameter.

In order for a particle to be properly sized by the OAP it must be neither too large nor too small and must pass within a well defined, drop size dependent region relative to the laser beam. Droplets outside these bounds will be ignored by the OAP. It is possible, therefore, that one or more of the

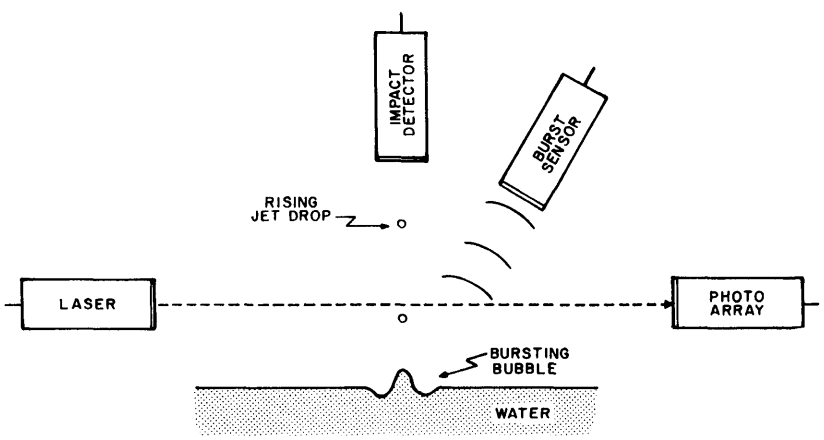

Fig. 1. Schematic showing the arrangement of sensors used to measure bursting bubble parameters.

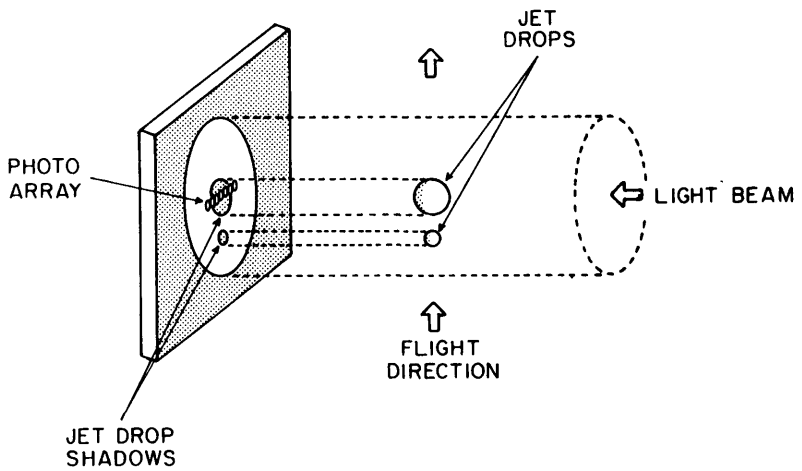

Fig. 2. Illustration of the method used by the OAP to determine drop size.

droplets in a train of droplets emitted from a bursting bubble will go unreported by the OAP even though there has been shadowing of the photoarray. It is also possible, of course, that a drop could miss the laser beam altogether and pass without any detection by the OAP. Techniques have been developed to assure that there are no "missed" droplets. There is within the OAP an electrical bus which responds whenever any of the photodetectors experiences at least a 50% reduction in incident light. This bus returns to normal when no photodetector is any longer shadowed. In effect, this shadow bus indicates the time when the leading edge of the particle passes a line, defined by the axis of the laser beam, and the time its trailing edge leaves this line somewhat later. If the particle passage satisfies the OAP's criteria, the OAP will enable a strobe of the data lines informing the computer that the data is on line (see Fig. 3). Otherwise, no strobe is generated and the particle event is ignored. It is the strobe pulse that initiates the OAP-Computer handshake. By monitoring the shadow bus and the strobe, which, if issued, follows the end of the shadow by about 9 μs, any unreported droplets can be detected. In addition, by comparing the response of the impact detector to the sequence of shadow signals one can detect particles that missed the laser beam altogether and consequently cast no shadow. It is always possible to relate the impact signals to earlier shadow signals (but not always vice versa). The duration of the shadow pulse along with the particle size can be used to calculate the speed of the particle.

Fig. 3 is a block diagram of the electronics used to monitor the bubble bursts and jet droplets. A clock signal was added to the data lines that carry size information from the OAP to the computer so that when the OAP strobed the size data it also told the computer the time of the event. This clock was reset to zero by a signal from the digital oscilloscope issued when the bubble burst was detected. So, after correcting for the 57 μs it took the Helmholtz signal to get from the bubble to the burst detector, the time reported for a given droplet was the elapsed time from the moment of burst to the moment the OAP issued its strobe of the data lines. The clock period of 10 μs was

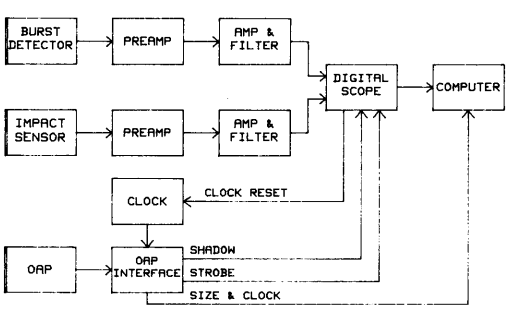

Fig. 3. Block diagram of the electronics used to measure bubble burst parameters.

adequate to assure absolutely which size reported by the OAP went with which signals recorded for the event.

The preamps shown in Fig. 3 are Ithaco model 568 low noise amplifiers which have a dc coupled input impedance of 5 G ohms, an 8 pf input capacitance, a 20 or 40 dB gain and a 10 MHz bandwidth. Amplification after the Ithacos, when required, was provided by Tektronix model AM502 amplifier-filters. They provide variable gains up to 10^5, variable low pass and/or high pass filtering and have a maximum bandwidth of 1 MHz. The digital oscilloscope is a Nicolet model 430 with two channels of differential input. It can sample up to 256 K samples per channel at up to 10 M samples/s with 12-bit resolution.

The same channel that recorded the Helmholtz signal, and thereby provided the $t = 0$ trigger, also recorded the shadow signals from the OAP which were input to the opposite differential input from the Helmholtz signal. Since the droplet transits which give rise to the shadow signals occur much later than the Helmholtz signal, there is no confusion in differentiating between the two signals on the same trace. The remaining channel, triggered by the first, recorded the impact sensor response and also had the strobe signals input to the opposing differential input. An example of these two traces is provided in Fig. 4. A bubble burst, then, resulted in two traces on the digital scope containing the Helmholtz burst signal, the shadow bus pulses, the strobes and the signals generated by the impact detector. At the same time, the OAP was telling the computer, in the order detected, the sizes of the particles and times of their strobes. Each acceptable event was recorded, for later analysis, on the internal mass storage of the Nicolet and on the computer's mass storage as well.

For the study of jet drop numbers and sizes reported here, the distance from the water surface to the center of the laser beam was between 2.6 and 3.1 mm depending upon bubble size. The impact sensor was an added 1 to 1.7 mm above the laser beam center. It was desirable that the laser beam pass as close to the bubble as possible in order to

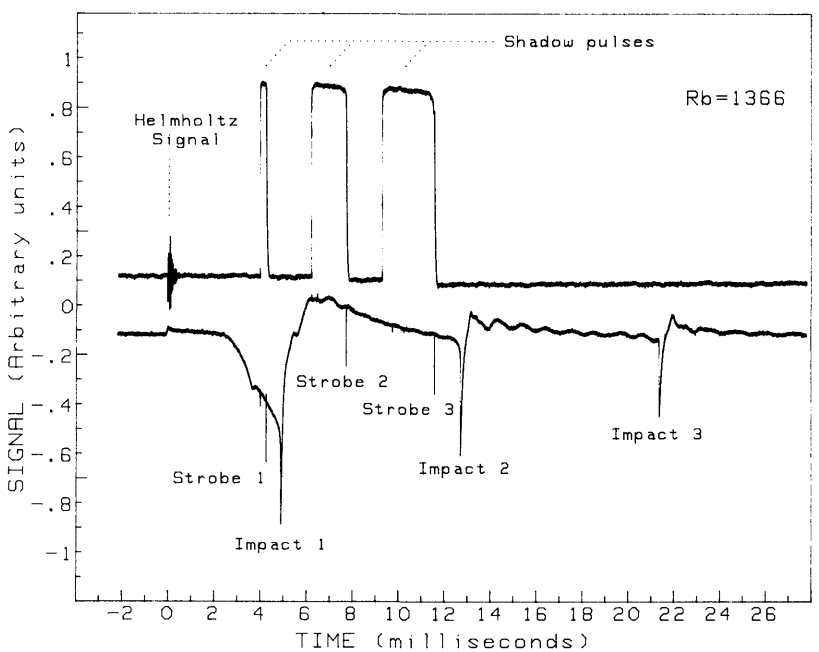

Fig. 4. An example of the dual traces on the digital oscilloscope combining the Helmholtz, shadow, strobe and impact detector signals resulting from a bubble collapse which produced at least three jet drops. The seawater bubble size was 1366 μm radius.

detect any of the droplets that might have low maximum trajectory heights. It was important, however, to place the laser at a height sufficient to assure that it was above the maximum excursion of the intact jet. Therefore, for each bubble size studied, this maximum jet height was measured.

This was accomplished with what was, in effect, an ohmmeter. An electrode at a potential of a few volts with respect to the water was lowered until continuity was detected when the jet rose from the collapsing bubble and touched the electrode. This simple technique can be used to measure such interesting jet parameters as its speed as a function of height, the height at which drops separate, and the resultant discontinuous changes in the jet tip speed after drop separations.

The impact signal shown in Fig. 4 was generated by capacitively coupling to the bursting bubble. If an electrode is placed directly over the collapsing bubble somewhat above the maximum excursion of the rising jet and raised to a potential of, say, 300 V, then one obtains a view of the whole bubble burst and collapse process from the sudden appearance of the cavity in the water, the rising jet, drop separations and finally the impacts of the droplets on the electrode which formed one side of the capacitor while the collapsing bubble and surrounding water formed the other. The jet drops carry an electrical charge, induced by the 300 volts, which when transferred to the impact detector provide a substantial signal as may be seen in Fig. 4.

The positioning of the bubble relative to the OAP's laser is critical. The sampling area of the OAP is droplet size dependent varying from 0.059 mm^2 for a 6 μm radius droplet to a peak of 28.67 mm^2 for an 80 μm drop and back down to 0.61 mm^2 for a 310 μm drop. In order to assure bubble position repeatability, the water surface was constrained to a diameter of 20 mm which gave rise to a modest, but adequate, meniscus. It was necessary, however, to have a bubble surface life of at least two seconds to assure that the bubble occupied the meniscus' apex over which the OAP's laser beam had been positioned. For seawater, the average surface life exceeded this limit so there was little problem with the bubble positioning itself before it burst. The fresh-water used, however, was very clean initially with a resistivity of the order of 10^7 Ω cm. When this water was first introduced into the apparatus bubbles usually burst immediately. These bubbles had relatively high Helmholtz frequencies, based upon their known size, indicating that they were bursting while above their equilibrium height. Usually, however, letting the surface "age" for 10 to 15 minutes was sufficient to alter the water's surface so that the bubble life increased to the required two or three seconds. During the course of a measurement sequence, the water's surface was replaced periodically by overflowing in which case it was again often, but not always, necessary to age the surface. The water was replaced whenever a new bubble size was started or daily, whichever came first. The apparatus containing the water and the bubblers used to create the bubbles was cleaned periodically as described earlier (Spiel, 1992). Distances between the water's surface and various detectors was measured by a cathetometer. The seawater, obtained in Monterey Bay, was filtered to remove particulates down to 2 μm radius.

The water that accumulated on the impact sensor during each bubble burst and subsequent collapse was removed by blotting before the next bubble was generated. It should be noted that only the top drop hits the impact sensor directly. All subsequent drops pile onto their predecessors and do not, therefore, have to travel quite as far before impacting. The data suggests that the pendants formed by the impinging droplets oscillate in shape after formation or when excited by newly arriving droplets. Given this oscillating pendant, it is difficult to know exactly how the accumulating water alters the distance each subsequent droplet must travel before impacting.

3. Results

For all of the results discussed here the temperature of the water was in the range 18 to 25°C. The range of size of bubbles used in this study was constrained by the limits of the OAP. Results are given for eleven bubble sizes, for each water type, in the range of about 350 to 1500 μm radius. No attempt was made to determine the surface chemistry responsible for the "aging" of the surface of the initially very clean fresh-water.

The probability, $p(n)$, that an nth drop was produced by a bubble of a given size, R_b, is listed in Table 1 for n up to 7. The number of bubbles in each sample, N_s, is also given there. The total

Table 1. *Probability that a bursting bubble with a radius R_b produces an nth jet drop*

R_b (μm)	$p(1)$	$p(2)$	$p(3)$	$p(4)$	$p(5)$	$p(6)$	$p(7)$	N_s	
349	1	1	1	0.97	0.66	0.40	0.01	76	F
345	1	1	1	0.85	0.69	0.05	0	80	S
500	1	1	1	0.80	0.30	0.07	0	73	F
490	1	1	1	1	0.75	0.33	0.08	72	S
563	1	1	1	0.83	0.27	0.09	0.05	78	F
559	1	1	1	0.97	0.91	0.17	0.01	77	S
636	1	1	1	0.60	0	0	0	80	F
630	1	1	1	0.99	0.88	0.32	0.03	74	S
732	1	1	1	0.62	0.30	0.15	0.01	74	F
727	1	1	0.98	0.93	0.25	0.08	0	80	S
817	1	1	0.69	0.68	0.17	0.05	0.04	78	F
811	1	1	1	0.50	0.10	0	0	80	S
917	1	1	0.49	0.14	0.03	0	0	79	F
911	1	1	0.84	0.14	0.06	0.03	0.01	80	S
1070	1	0.98	0.05	0.01	0.01	0.01	0	79	F
1017	1	0.91	0.74	0.11	0.06	0.03	0.03	80	S
1215	1	0.51	0.27	0.16	0.14	0.10	0.05	80	F
1212	1	0.63	0.18	0.11	0.08	0.06	0.05	80	S
1363	1	0.58	0.22	0.03	0.01	0.01	0	76	F
1366	1	0.26	0.04	0.01	0.01	0	0	80	S
1479	1	0.86	0.44	0.20	0.15	0.10	0.06	79	F
1471	1	0.45	0.11	0.04	0.01	0	0	80	S

N_s is the number of bubbles in the sample. F indicates fresh-water and S indicates seawater.

number of bubble bursts listed in Table 1 (the sum of the N_s column) is 1715 combining sea- and fresh-water data. Twenty of these bubble bursts (1.2%) yielded more than seven droplets and four of them ($\simeq 0.2\%$) resulted in at least 15 jet drops. 15 was the limit, set in software, of the number of droplets that could be recorded for a single event. Evidence has been given (Spiel, 1992) that a burst could, on occasion, result in a train of numerous closely spaced jet droplets flying as if in information. Such clusters have been detected by the OAP in this study as well. In a private communication, Duncan Blanchard said that he has visually observed just such formations.

There are some peculiar variations of $p(n)$ with R_b, especially for $n = 6$, evident in Table 1. For example, the probability of the generation of a sixth drop in seawater is 0.5, 0.33, 0.17, 0.32 and 0.08 as the bubble size varies from 345 to 727 μm. This is a statistically significant variation for which there is yet no explanation. Perhaps an analysis of the ejection speeds and energetics as a function of bubble size, for which the data is now available, will afford some insight.

The size distributions for the jet drops produced by collapsing bubbles are presented in Figs. 5 and 6 for fresh-water and Figs. 7 and 8 for seawater. These histograms show, for the top six droplets in sequence, the number of jet drops with radii within ± 2.5 μm of R_d, the radius bin center, produced by the $N_s(R_b)$ collapsing bubbles. The vertical ticks extending just below the abscissa in each of these figures are the size bin edges. The number between pairs of these bin edges is the bin center size. The number in the upper right corner of each histogram is n. Here $n = 1$ is the top drop, the first to be emitted, $n = 2$ is the second drop and so on. These histograms show that for $n > 1$ the size distributions are often bimodal for both types of water. It is evident from this data that the variance in R_d increases with both R_b and n.

The average droplet size as a function of bubble size, for n up to 5, is plotted in Fig. 9. Where the distributions were clearly bimodal, two averages have been calculated and plotted separately. Values were plotted only if there were more than five data points to contribute to the average. The results for the top drop are in agreement with the earlier results for seawater published by Blanchard (1989) as illustrated in Fig. 9. Regression fits of the R_d versus R_b data show no statistically significant differences between the two water types. Combining the two data sets is therefore justified and has been done in calculating fits for each of the first 5 drops. Excluding the droplets comprising the modes of smaller drops, regression fits for each of these 5 jet drops show that whereas the second through fifth drops are statistically indistinguishable, they are different from the top drop. For the equation $R_d = \alpha R_b^{\kappa}$, the follwing values were derived for radii (μm):

	α	κ
top drop	0.0337 ± 0.0007	1.208 ± 0.003
second through 5th	0.0165 ± 0.0006	1.325 ± 0.006

These fits are shown as the solid lines in the plots of Fig. 9. The points for the 2nd and 3rd drops for bubbles larger than 1300 μm are shown as belong-

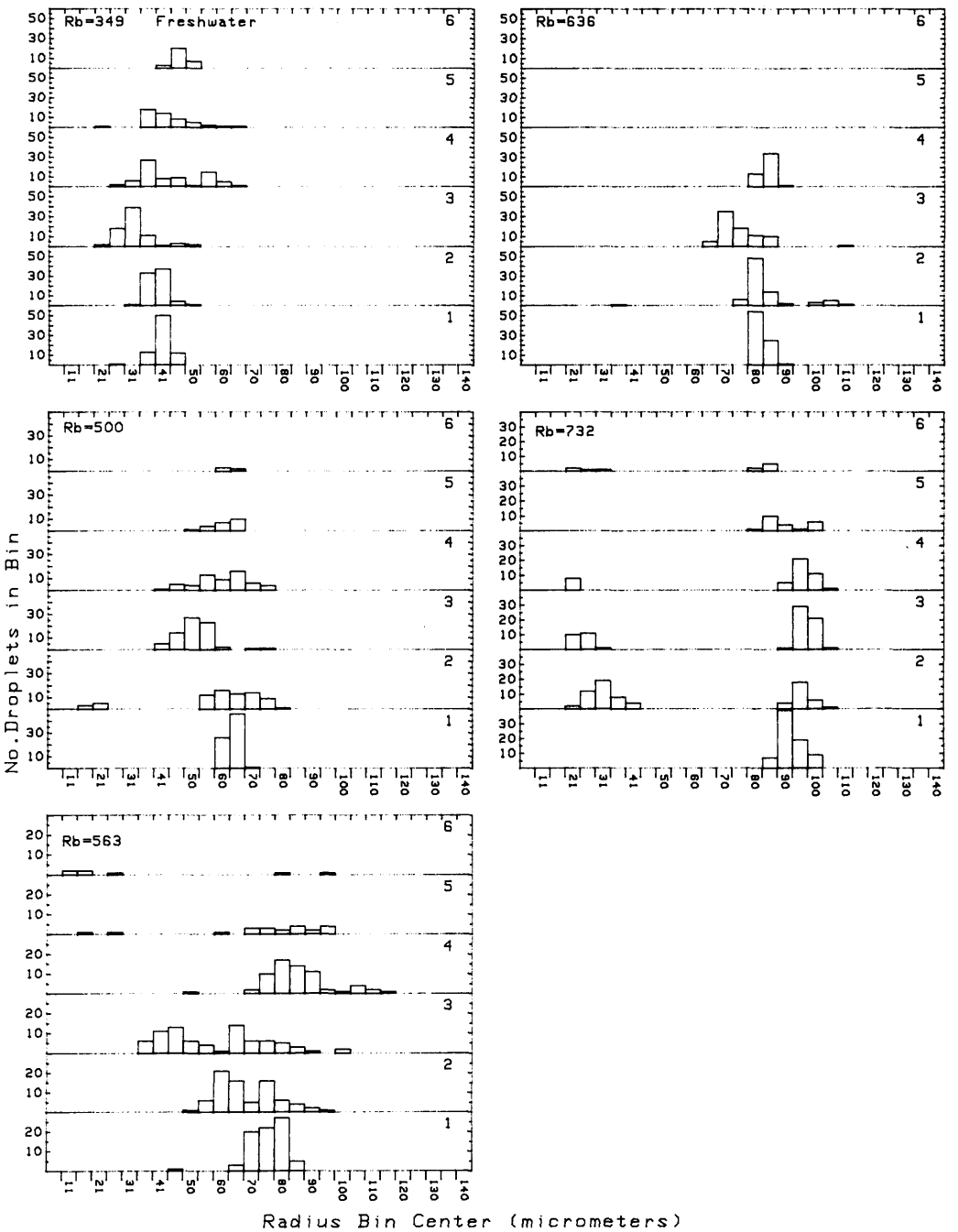

Fig. 5. Histograms of the number of jet drops of a given size produced by collapsing bubbles with radii of 349, 500, 563, 636 and 732 μm in fresh-water. The vertical tick marks extending below the abscissa are the edges of the size bins and the numbers between those bin edges are the bin center sizes.

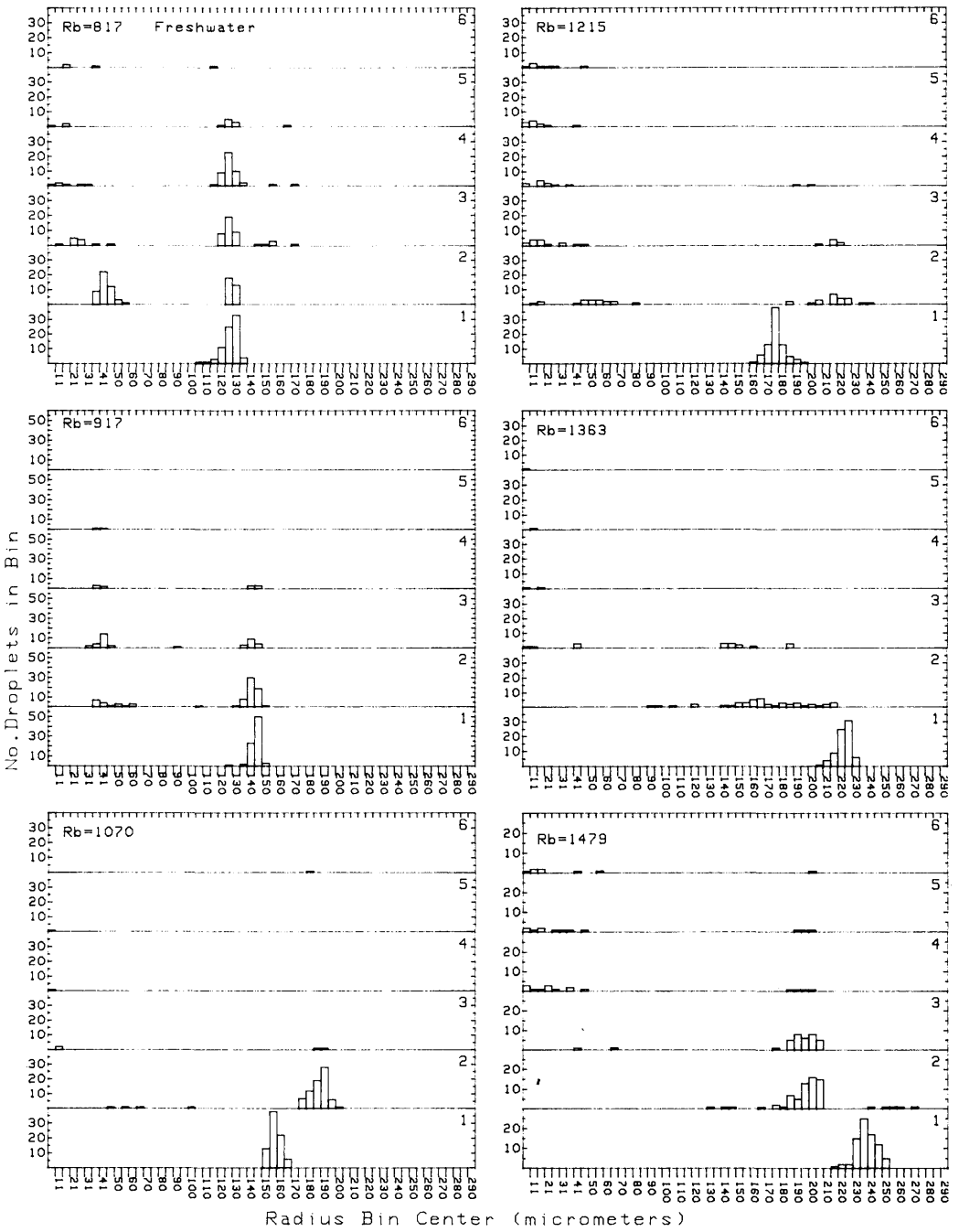

Fig. 6. Histograms of the number of jet drops of a given size produced by collapsing bubbles with radii of 817, 917, 1070, 1215, 1363 and 1479 μm in fresh-water.

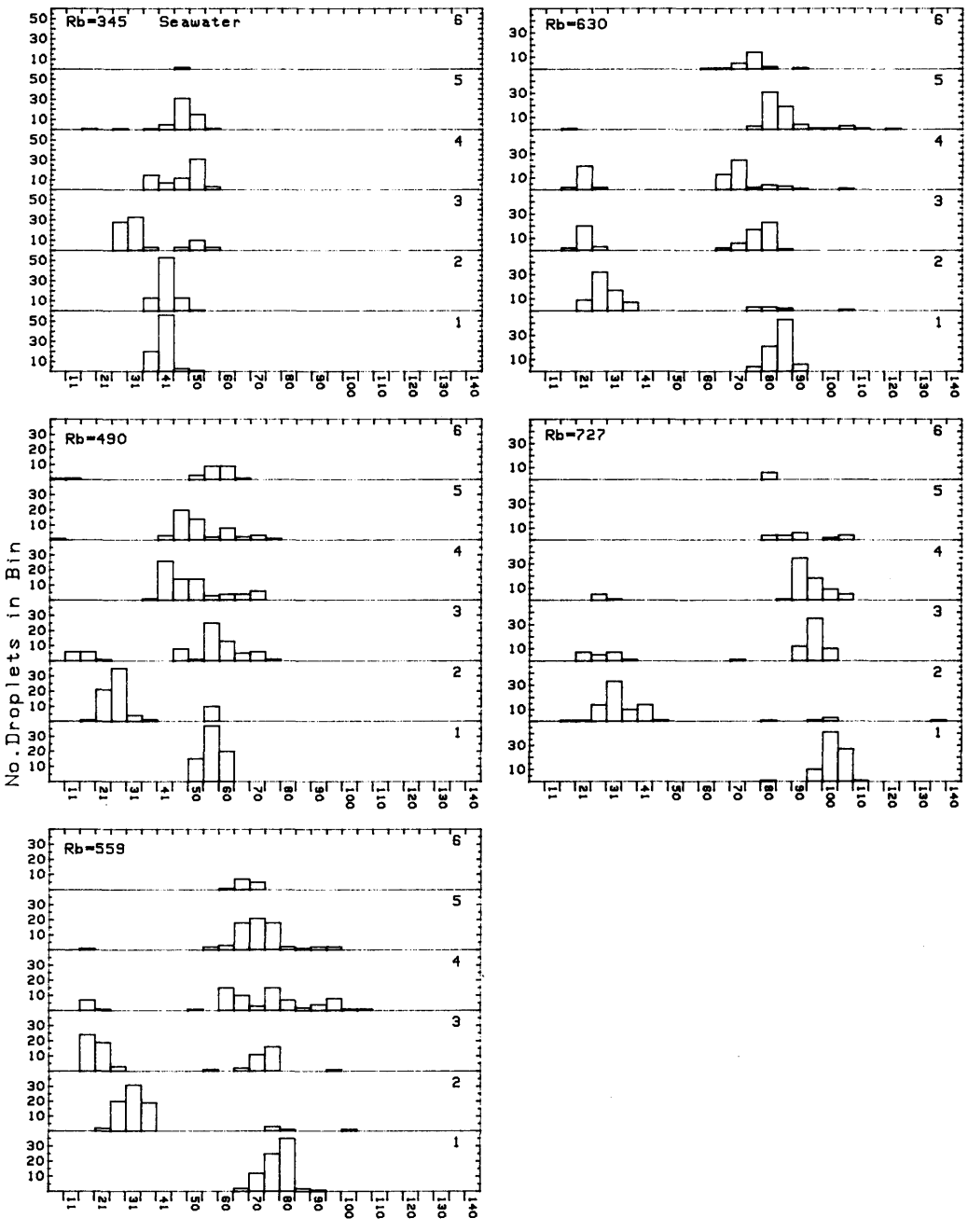

Fig. 7. Histograms of the number of jet drops of a given size produced by collapsing bubbles with radii of 345, 490, 559, 630 and 727 μm in seawater.

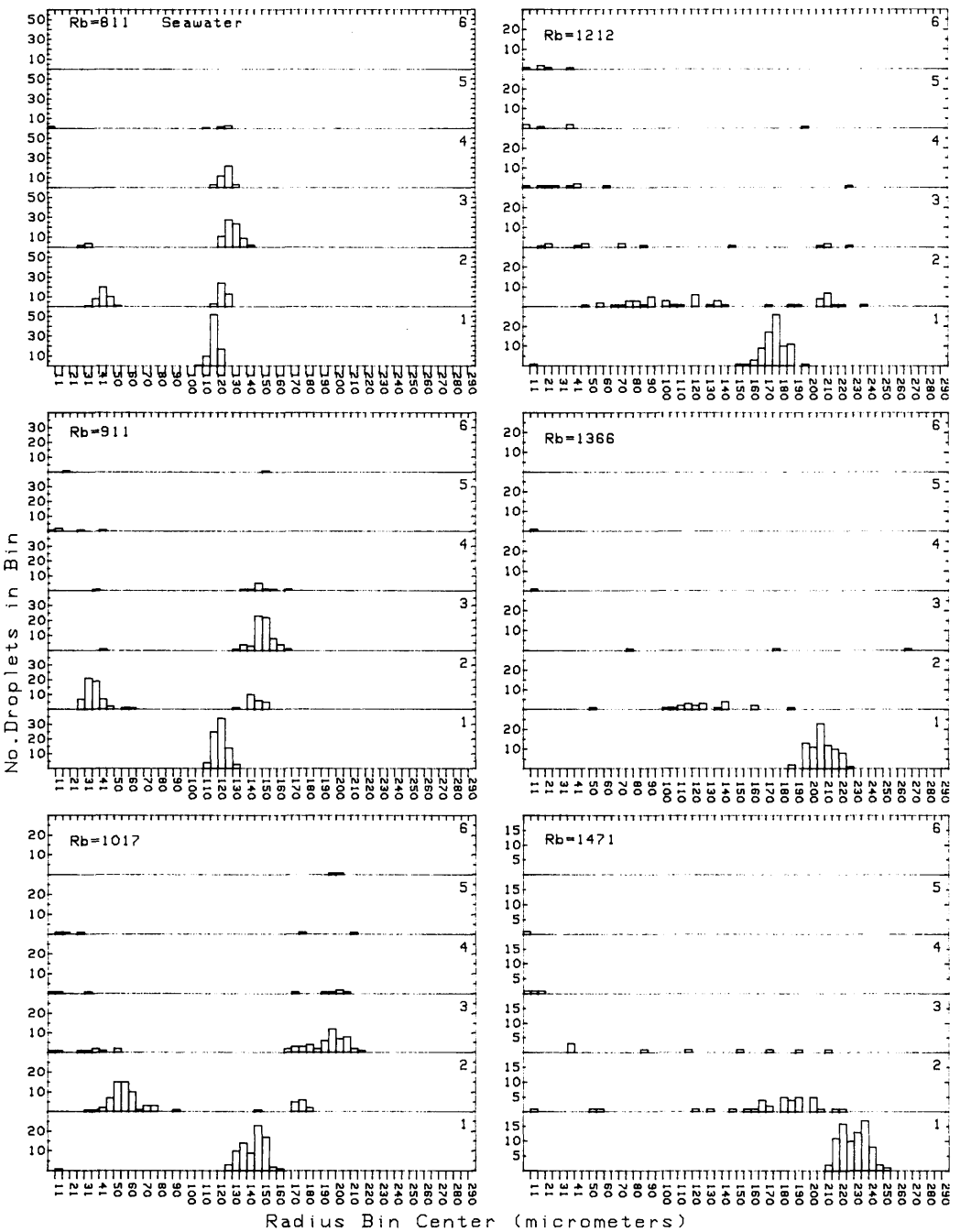

Fig. 8. Histograms of the number of jet drops of a given size produced by collapsing bubbles with radii of 811, 911, 1017, 1212, 1366 and 1471 μm in seawater.

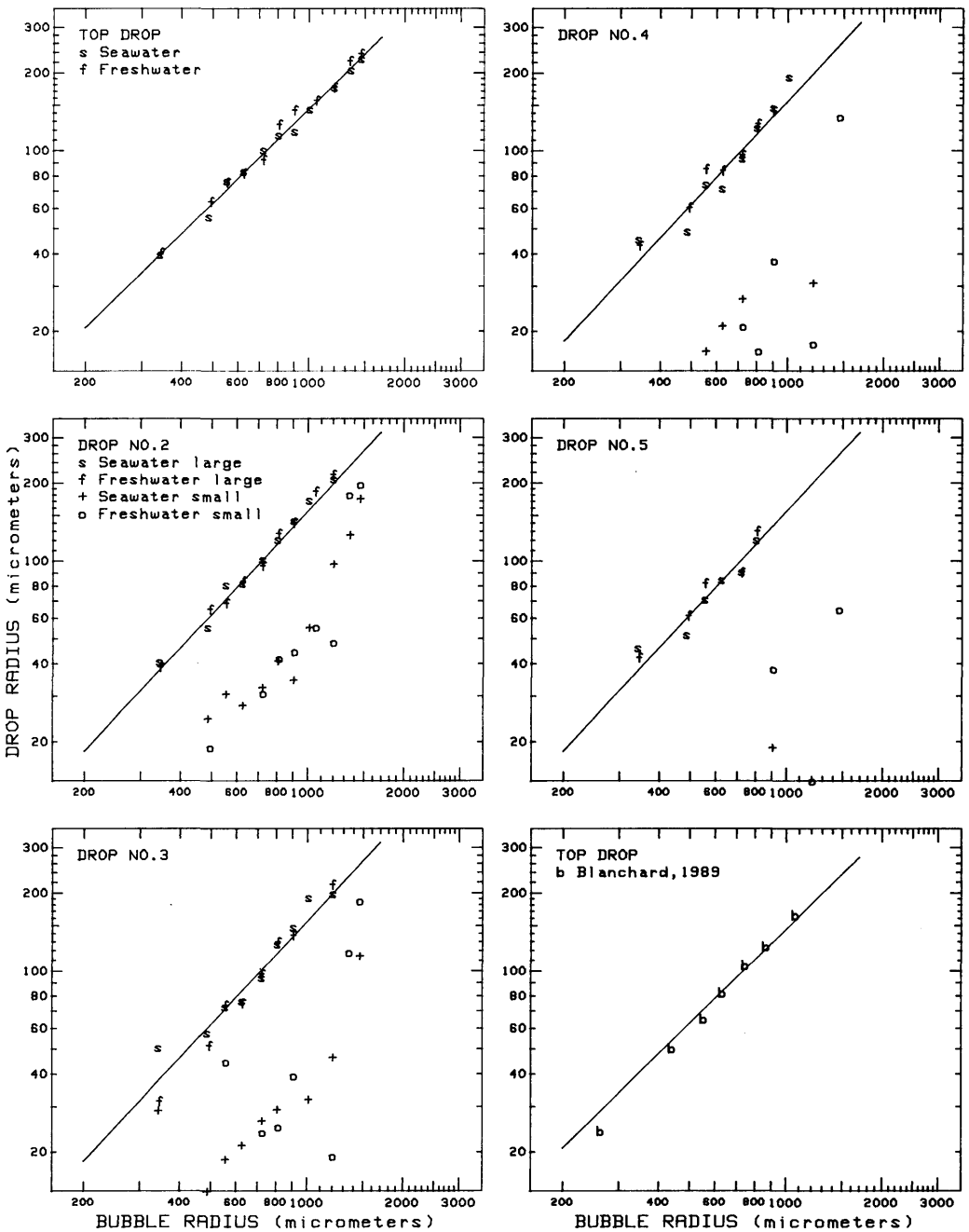

Fig. 9. Plots of the average jet drop size as a function of bubble size for drop numbers up to five. The fits to the data for the top and lower drops from the larger modes are given by the solid lines. The drop size dependence on bubble size is the same for the second through fifth large-mode drops, within statistical certainty, but is different from the top drop, see the text. Blanchard's results for the top drop are compared to current results in a separate plot to avoid congestion.

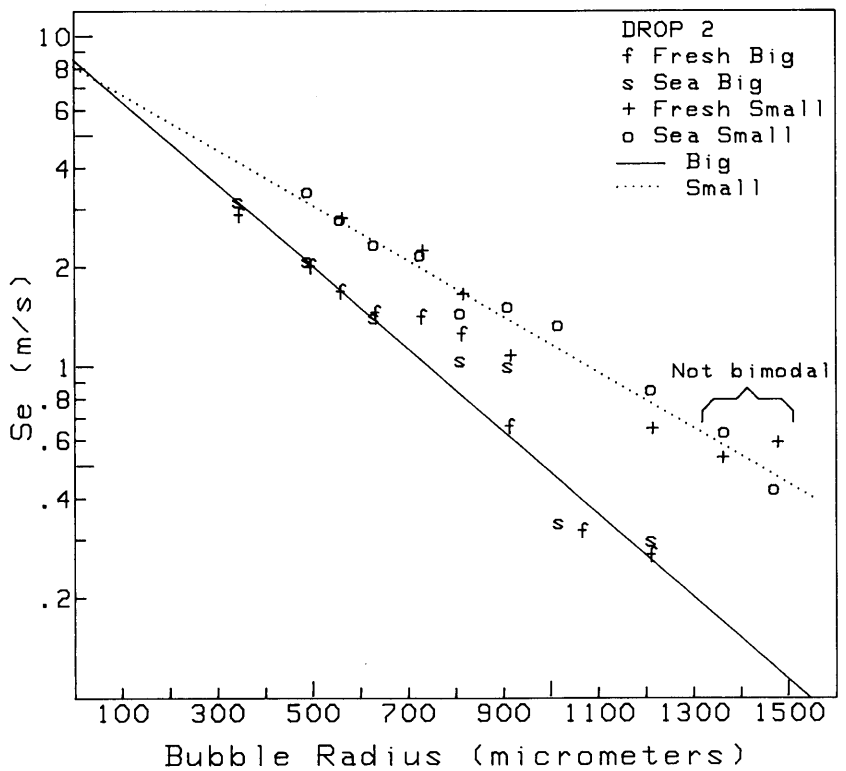

Fig. 10. The average ejection speed, Se, of drop 2 as a function of parent bubble size. The size mode of the droplets has been used as a parameter to illustrate that the droplets observed from bubbles larger than 1300 μm belong to the mode of smaller droplets.

ing to the mode of smaller sizes even though the distributions are not bimodal and would appear, with no other evidence, to belong to the mode of larger droplets. That these droplets should be classified as belonging to the mode of smaller droplets is demonstrated, however, by a plot of droplet ejection speeds as a function of bubble radius with the two size modes as parameters as illustrated, for example, in Fig. 10. The droplet size distributions for bubbles larger than 1300 μm for both water types are not significantly bimodal as can be seen in Figs. 6, 8. It is possible that larger drops were created, but had insufficient energy to reach the OAP beam. Note that their average ejection speeds would have been less than 0.2 m/s. Clearly, those droplets that were seen should be classified as belonging to the mode of small droplets based on their ejection speeds, Se, as shown in Fig. 10. Details of the measurement of ejection speeds and the resulting data will be published later.

No fits are provided for the droplets comprising the smaller modes. They are not well fit by a simple power law; in fact, an exponential fit works better, but the rules for assigning a droplet or group of droplets to one mode or another are not now well defined and may, in the end, for that matter, not even be useful. Much more work needs to be done to understand the distributions of droplet sizes.

4. Summary and plans

Data showing the number and size of the jet drops produced by bubbles with radii from 350 to 1500 μm has been presented. There does not appear to be any significant difference in the results between sea- and fresh-water for bubbles of the

sizes reported here. Blanchard (1963), however, reported differences between jet drops produced by distilled water and seawater for smaller bubbles. Except for the top drop, the size distributions are often bimodal. For the larger droplets a simple power law equation suffices to describe the droplet size dependence on parent bubble size. For these larger drops, the top drop size variation with bubble size is different from the second through fifth drops all the latter of which, however, appear to have identical size dependences on bubble size. No such simple fit works for the smaller droplets. Calculations of jet drop ejection speeds for the range of bubble sizes reported on here are currently underway.

5. Acknowledgements

This work was supported by the Office of Naval Research Code 1241 (Air–sea Boundary Layers Program). I gratefully acknowlede the contributions of Gerrit De Leeuw, Patrice Mestayer and Gary Geernaert who have offered valuable advice. George Jaksha and Steve Blankschein were quite helpful in the design and construction of some of the apparatus used in these measurements.

REFERENCES

Afeti, G. M. and Resch, F. J. 1990. Distribution of the liquid aerosol produced from bursting bubbles in sea and distilled water. *Tellus* **42B**, 378–384.

Blanchard, D. C. 1958. Electrically charged drops from bubbles in seawater and their meteorological significance. *J. Meteor.* **15**, 383–396.

Blanchard, D. C. 1963. The electrification of the atmosphere by particles from bubbles in the sea. *Progr. Oceanogr.* **1**, 71–202.

Blanchard, D. C. 1983. The production, distribution, and bacterial enrichment of the sea-salt aerosol. In: *The air–sea exchange of gases and particles* (ed. P. S. Liss and W. G. N. Slinn). D. Reidel, Hingham, Mass., 407–454.

Blanchard, D. C. 1989. The size and height to which jet drops are ejected from bursting bubbles in seawater. *J. Geophys. Res.* **94**, 10999–11002.

Blanchard, D. C. 1990. Surface-active monolayers, bubbles, and jet drops. *Tellus* **42B**, 200–205.

Blanchard, D. C. and Syzdek, L. D. 1972. Concentration of bacteria in jet drops from bursting bubbles. *J. Geophys. Res.* **27**, 5087–5098.

Blanchard, D. C. and Syzdek, L. D. 1975. Electrostatic collection of jet and film drops. *Limnol. Oceanogr.* **20**, 762–774.

Blanchard, D. C. and Syzdek, L. D. 1988. Film drop production as a function of bubble size. *J. Geophys. Res.* **93**, 3649–3654.

Blanchard, D. C. and Woodcock, A. H. 1957. Bubble formation and modification in the sea and its meteorological significance. *Tellus* **9**, 145–158.

Burk, S. D. 1984. The generation, turbulent transfer and deposition of the sea-salt aerosol. *J. Atmos. Sci.* **41**, 3040–3051.

Coantic, M. 1980. Mass transfer across the ocean-air interface: small scale hydrodynamic and aerodynamic mechanisms. In: *Physico-chemical hydrodynamics*, vol. 1. Pargamon, Elmsford, New York, 249–279.

Coantic, M., Ramanonjiarisoa, A., Mestayer, P., Resch, F. and Favre, A. 1981. Wind-water tunnel simulation of small-scale ocean-atmosphere interactions. *J. Geophys. Res.* **86**, 6607–6627.

Day, J. A. 1964. Production of droplets and salt nuclei by the bursting of air bubble films. *Quart. J. Roy. Met. Soc.* **90**, 72–78.

Dekker, H. and De Leeuw, G. 1993. Bubble excitation of surface waves and aerosol droplet production: a simple dynamical model. *J. Geophys. Res.* **98**, 10223–10232.

De Leeuw, G. 1987. Near-surface particle size distribution profiles over the North sea. *J. Geophys. Res.* **92**, 14631–14635.

De Leeuw, G. 1991. Aerosols models for optical and IR propagation in the marine atmospheric boundary layer. *Proc. SPIE Int. Soc. Opt. Eng.* **1487**, 15-1 to 15-30.

Detwiler, A. and Blanchard, D. C. 1978. Aging and bursting bubbles in Trace-contaminated water. *Chem. Eng. Sci.* **33**, 9–13.

Katsaros, K. B., Smith, S. D. and Oost, W. A. 1987. HEXOS, A program for research on water-vapor and droplet fluxes from sea to air at moderate to high wind speeds. *Bull. A, Meteorol. Soc.* **68**, 466–476.

Kerman, B. R. 1984. A model of interfacial gas transfer for a well-roughened sea. *J. Geophys. Res.* **89**, 1439–1446.

Kientzler, A. B., Arons, A. B., Blanchard, D. C. and Woodcock, A. H. 1954. Photographic investigation of the projection of droplets by bubbles bursting at a water surface. *Tellus* **6**, 1–7.

Laţsen, S. E., Edson, J. B., Mestayer, P. G., Fairall, C. W. and De Leeuw, G. 1990. Sea spray and particle deposition: Air–sea tunnel experiment and its relation to over-sea conditions. In: *The Proceedings of Eurotrac Symposium '90* (ed. P. Borel et al.). Academic Publishing, The Hague, Netherlands, 71–77.

MacIntyre, F. 1972. Flow patterns in breaking bubbles. *J. Geophys. Res.* **77**, 5211–5228.

Merlivat, L. and Memery, L. 1983. Gas exchange

across an air–water interface: experimental results and modeling of bubble contribution to transfer. *J. Geophys. Res.* **88**, 707–724.

Mestayer, P. G. and Lefauconnier, C. 1988. Spray droplet generation, transport, and evaporation in tunnel during humidity exchange over the Sea experiments in simulation tunnel. *J. Geophys. Res.* **93**, 572–586.

Mestayer, P. G., Edson, J. B., Fairall, C. W., Larsen, S. E. and Spiel, D. E. 1989. Turbulent transport and evaporation of droplets generated at an air–water interface. In: *Turbulent shear flows*, vol. 6 (ed. J. C. Andre et al.). Springer-Verlag, New York, 129–147.

Monahan, E. C. and Spillane, M. C. 1984. The role of oceanic whitecaps in air–sea exchange. In: *Gas Transfer at water surfaces* (ed. W. Brutsaert and G. H. Jirke). D. Reidel, Hingham, Mass., 459–503.

Resch, F. J., Darrozes, J. S. and Afeti, G. M. 1986. Marine liquid aerosol production from bursting air bubbles. *J. Geophys. Res.* **91**, 1019–1029.

Resch, F. and Afeti, G. 1991. Film drop distributions from bubbles bursting in seawater. *J. Geophys. Res.* **96**, 10681–10688.

Resch, F. and Afeti, G. 1992. Submicron film drop production by bubbles in seawater. *J. Geophys. Res.* **97**, 3679–3683.

Rouault, M. P., Mestayer, P. G. and Schiestel, R. 1991. A model of evaporating spray droplet dispersion. *J. Geophys. Res.* **96**, 7181–7200.

Schacher, G. E., Davidson, K. L., Fairall, C. W. and Spiel, D. E. 1981. Calculation of optical extinction from aerosol spectral data, *Appl. Optics* **20**, 3951–3957.

Spiel, D. E. 1992. Acoustical measurements of air bubbles bursting at a water surface: bursting bubbles as Helmholtz resonators. *J. Geophys. Res.* **97**, 11443–11452.

Stramska, M. 1987. Vertical profiles of sea-salt aerosol in the atmospheric surface layer: a numerical model. *Acta Geophys. Pol.* **35**, 87–100.

Toba, Y. 1959. Drop production by bursting of air bubbles on the sea surface (II). Theoretical study on shape of floating bubbles. *J. Ocean. Soc. Jap.* **15**, 1–10.

Woodcock, A. H. 1952. Atmospheric salt particles and raindrops. *J. Meteo.* **9**, 200–212.

Woodcock, A. H. 1953. Bursting bubbles and air pollution. *Sewage and Industrial Wastes* **27**, 1189–1192.

Woodcock, A. H., Kientzler, C. F., Arons, A. B. and Blanchard, D. C. 1953. Giant condensation nuclei from bursting bubbles. *Nature* **172**, 1144–1145.

Printed in Belgium